Structural Engineering and Mechanics, *Vol. 53, No. 2 (2015) 227-248*
DOI: http://dx.doi.org/10.12989/sem.2015.53.2.227

Base isolation performance of a cone-type friction pendulum bearing system

Bub-Gyu Jeon, Sung-Jin Chang, Sung-Wan Kim and Nam-Sik Kim*

Department of Civil & Environmental Engineering, Pusan National University, 30 Jangjeon-dong, Geumjeong-gu, Busan 609-735, Republic of Korea

(Received June 1, 2013, Revised May 7, 2014, Accepted May 9, 2014)

Abstract. A CFPBS (Cone-type Friction Pendulum Bearing System) was developed to control the acceleration delivered to a structure to prevent the damage and degradation of critical communication equipment during earthquakes. This study evaluated the isolation performance of the CFPBS by numerical analysis. The CFPBS was manufactured in the shape of a cone differenced with the existing FPS (Friction Pendulum System), and a pattern was engraved on the friction surface. The natural frequencies of the CFPBS were evaluated from a free-vibration test with a seismic isolator system consisting of 4 CFPBS. To confirm the earthquake-resistant performance, a numerical analysis program was prepared using the equation of the CFPBS induced from the equations of motion. The equation reported by Tsai for the rolling-type seismic isolation bearings was proposed to design the equation of the CFPBS. Artificial seismic waves that satisfy the maximum earthquake scale of the Korean Building Code-Structural (KBC-2005) were created and verified to review the earthquake-resistant performance of the CFPBS by numerical analysis. The superstructural mass of the CFPBS and the skew angle of friction surface were considered for numerical analysis with El Centro NS, Kobe NS and artificial seismic waves. The CFPBS isolation performance evaluation was based on the numerical analysis results, and comparative analysis was performed between the results from numerical analysis and simplified theoretical equation under the same conditions. The validity of numerical analysis was verified from the shaking table test

Keywords: cone-type friction pendulum bearing; friction pendulum system; seismic performance; seismic isolation; shaking table test

1. Introduction

The Northridge Earthquake (1994), Kobe Earthquake (1995) and other recent large-scale earthquakes have caused billions of dollars of damage to power and communication equipment in major cities (Murota *et al*. 2005, Japan Electric Association 1999). This damage can hinder emergency measures and functional recovery of damaged areas due to the suspension of power supply and damage of communication devices after an earthquake. During an earthquake, the major damage to a large communication device involves damage to the internal parts of communication devices by the transfer of an earthquake impact load due to the excessive

*Corresponding author, Professor, E-mail: nskim@pusan.ac.kr

http://www.techno-press.org/?journal=sem&subpage=8 ISSN: 1225-4568 (Print), 1598-6217 (Online)

anchorage or damage to anchorage device that fixes the main body. In addition, the device can turn over if the communication device is not anchored or is unstable. Therefore, it is essential to enhance the seismic performance by applying a seismic isolation system at the lower part of major communication devices and reduce the internal damage to communication devices by minimizing the impact load from an earthquake by isolating the major communication devices from earthquakes.

Among the various seismic isolation system, FPS (Friction Pendulum System) was proposed by Zayas *et al*. (1987), and Mokha *et al*. (1990). The FPS is a seismic isolation system used widely to isolate the building structure, communication devices and electronic devices from earthquakes. Jang *et al*. (2008) developed a FPS that can prevent the overturn of upper structures and reduce the response displacement by applying a shear key, rubber pad and uplift restrainer to a transformer. Hwang *et al*. (2008) examined a FPS that uses magnetism, which can enhance the seismic isolation performance by replacing the properties of materials with the repulsive power of the magnetic force. The FPS is a seismic isolation system that isolates the structure from an earthquake using the characteristics of a pendulum, and can determine the unique frequency of the structure by designing the curvature radius, angle of inclination and friction with a frictional surface for the friction panel, and accordingly reduce the response due to seismic motion.

An isolation method using free-rolling rods under the basement of structures was proposed by Lin and Hone (1993). Also, A sloped rolling-type bearing (RTB), which utilizes the concept of a steel cylinder rolling on a V-shape surface, has been proposed (Lee *et al.* 2003, Wu *et al.* 2004). Tsai *et al.* (2007) investigated performance of RTB by using seismic table tests. The dynamic behavior of a rolling-ball bearing which consists of a steel ball sandwiched between two conical steel load plates, has been studied and tested (Kasalanati *et al.* 1997, Kesti *et al.* 2010, Nacamuli *et al.* 2011). effectiveness of double concave Friction Pendulum Bearings and effect of soil-structure interaction for a building isolated with FPS was studied by Sevket (2012), Krishnamoorthy (2013) respectively.

In this study, the slope of the friction surface designed as a cone-type with a geometrical pattern was used to develop a CFPBS that can control the acceleration response and displacement response by earthquakes, confirm its performance through a shaking table test and dynamic numerical analysis, and propose a design equation.

2. Theoretical background

To evaluate the seismic performance of CFPBS, a theoretical equation based on a MATLAB 7.0-based numerical analysis program was established from the motion equation. Fig. 1 shows the pattern of the CFBPS friction surface and aseismic device composed of 4 CFPBS's. Fig. 2 shows the CFPBS during an earthquake load application, where the motion equation can be drawn from Fig. 2, as shown in Eq. (1), where m is the mass, c is the reductive coefficient, k is stiffness, $u(t)$ is the relative displacement, $\ddot{u}(t)$ is the relative acceleration, and $\ddot{u}_g(t)$ is the ground acceleration.

$$m\left(\ddot{u}(t)+\ddot{u}_g(t)\right)+c\dot{u}(t)+ku(t)=0 \tag{1}$$

For the CFPBS, there is no viscosity reduction and hardness, and friction and gravity work. Therefore, a free-body diagram like Fig. 3 can be drawn, and the motion Eq. (2) could be found. Eq. (3) shows the vertical load of the slope. Substituting Eq. (3) into Eq. (2) leads to Eq. (4). By

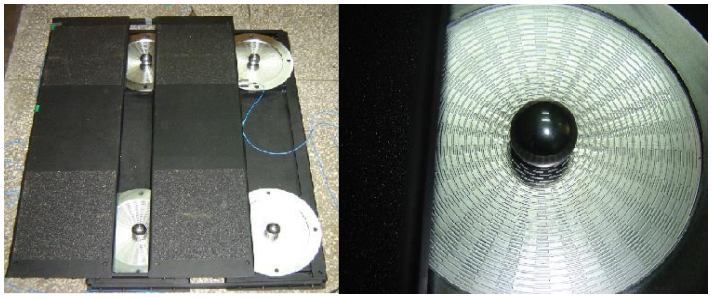

Fig. 1 Aseismic device composed of 4 CFPBS's(Cone-type Friction Pendulum Bearing System)

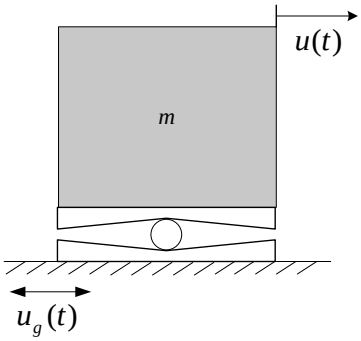

Fig. 2 Conceptual diagram of the CFPBS

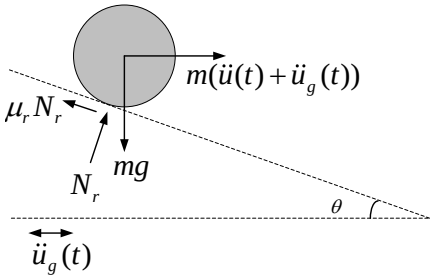

Fig. 3 Free-body diagram of the CFPBS

expressing Eq. (4) as a motion equation for force during time, Δt, it can be expressed as Eq. (5) (Jeon *et al*. 2011), where μ_r is the ratio of the ball radius to the cloud friction coefficient and θ is the slope angle of the CFPBS.

$$m\ddot{u}(t)+\mu_r N_r\cos\theta\,\mathrm{sgn}\left(\dot{u}(t)\right)+N_r\sin\theta\,\mathrm{sgn}\left(u(t)\right)=-m\ddot{u}_g(t) \tag{2}$$

$$N_r=m\left(g-\ddot{u}_g(t)\tan\theta\,\mathrm{sgn}(x)\right)\cos\theta \tag{3}$$

$$\begin{aligned}&m\ddot{u}(t)+\mu_r mg\cos^2\theta\,\mathrm{sgn}\left(\dot{u}(t)\right)-\mu_r m\ddot{u}_g(t)\sin\theta\cos\theta\,\mathrm{sgn}\left(u(t)\right)\mathrm{sgn}\left(\dot{u}(t)\right)\\&+mg\cos\theta\sin\theta\,\mathrm{sgn}\left(u(t)\right)-m\sin^2\theta\ddot{u}_g(t)=-m\ddot{u}_g(t)\end{aligned} \tag{4}$$

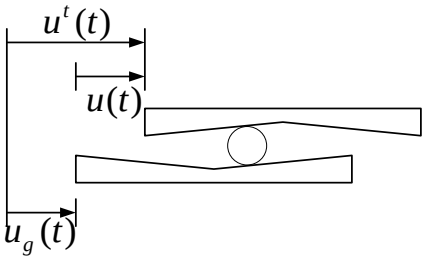

Fig. 4 Calculation of the displacements

$$\begin{aligned} &m\Delta\ddot{u}_{i+1} + \mu_r mg\cos^2\theta\,\mathrm{sgn}(\dot{u}_i) - \mu_r m\Delta\ddot{u}_{gi+1}\sin\theta\cos\theta\,\mathrm{sgn}(u_i)\mathrm{sgn}(\dot{u}_i) \\ &+mg\cos\theta\sin\theta\,\mathrm{sgn}(u_i) - m\sin^2\theta\Delta\ddot{u}_{gi+1} = -m\Delta\ddot{u}_{gi+1} \end{aligned} \tag{5}$$

The changes in the relative displacement, relative velocity and relative acceleration defined in Newmark-β method can be expressed as Eqs. (6), (7) and (8).

$$\Delta u_i = \frac{\Delta t^2}{6}\Delta\ddot{u}_i + \Delta t\dot{u}_i + \frac{\Delta t^2}{2}\ddot{u}_i \tag{6}$$

$$\Delta\dot{u} = \frac{\Delta t}{2}\Delta\ddot{u}_i + (\Delta t)\dot{u}_i \tag{7}$$

$$\Delta\ddot{u}_i = \frac{6}{\Delta t^2}\Delta u_i - \frac{6}{\Delta t^2}\Delta\dot{u}_i - 3\ddot{u}_i \tag{8}$$

The mass (m) can be found from the load to apply to the bearing, and μ_r is an arbitrary value. For an initial relative displacement, relative velocity and relative acceleration of 0, the seismic load ($m\Delta\ddot{u}_{gi}$) is used to apply a free vibration. In such cases, the relative acceleration response relative velocity response and relative displacement response are found from Eqs. (8), (7) and (6), respectively. The acceleration response, velocity response, and displacement response from Eqs. (6), (7) and (8) are the relative responses of the lower panel and upper panel of the bearing. On the other hand, an absolute response is necessary for seismic response analysis. As confirmed in the CFPBS (Fig. 4), the absolute response was determined using Eqs. (9), (10) and (11). Here, $u(t)$ is the absolute displacement response, $\dot{u}^t(t)$ is the absolute velocity response, and $\ddot{u}^t(t)$ is the absolute acceleration response.

$$u^t(t) = u_g(t) + u(t) \tag{9}$$

$$\dot{u}^t(t) = \dot{u}_g(t) + \dot{u}(t) \tag{10}$$

$$\ddot{u}^t(t) = \ddot{u}_g(t) + \ddot{u}(t) \tag{11}$$

$$\mu_r mg\cos^2\theta - \mu_r m\ddot{u}_g(t)\sin\theta\cos\theta + mg\cos\theta\sin\theta - m\sin^2\theta\ddot{u}_g(t) \tag{12}$$

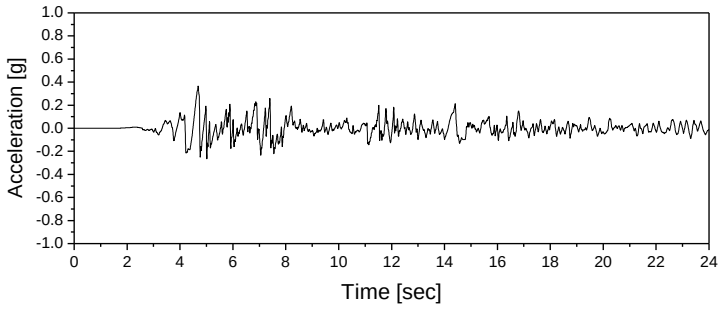

Fig. 5 Time history of El Centro(NS component, 1940), PGA=0.348g

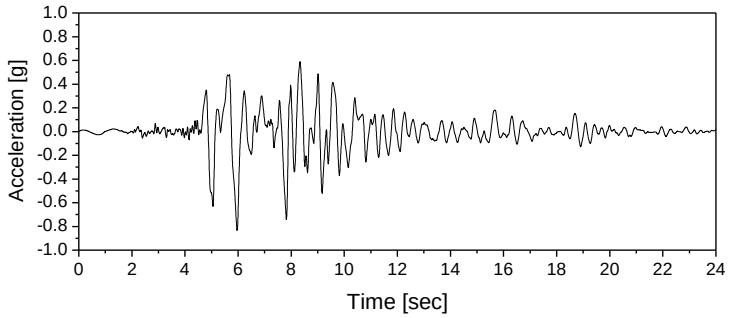

Fig. 6 Time history of Kobe(NS component, 1995), PGA=0.835g

3. Input seismic wave

Among the representative seismic waves actually measured in the past, those with high utility for seismic analysis due to the comprehensive frequency characteristics of the acceleration response, as in Figs. 5 and 6, such as El Centro NS (NS component, 1940, PGA=0.348g) and Kobe NS(NS component, 1995, PGA=0.835g), which greatly damaged Japan, were used as the input seismic waves to evaluate the seismic performance of CFPBS.

The Korean Building Code-Structural (KBC-2005) (Architectural Institute of Korea 2005) suggests the design response spectrum shown in Fig. 8, and this report created and used seven artificial seismic waves that satisfy it. To create an artificial seismic wave, the trapezoid-shaped envelope function of ASCE 4-98 (American Society of Civil Engineers 1999) shown in Fig. 7 was used. To determine the coefficient representing the characteristics of the envelope function, the values of magnitude 7.0-7.5 were used by referring to Table 1. Fig. 9 shows a comparison of the design response spectrum and acceleration signal and response acceleration spectrum for one of the produced artificial seismic waves. The artificial seismic wave was amplified up to 1~3 fold to observe the response change in the CFPBS according to the amplification of the seismic wave with the same response spectrum.

According to the aseismic design specifications of Korea, the correlation coefficient of two input earthquakes, as shown in Eq. (13), were under 0.3 when seismic response analysis was performed by simultaneously applying the seismic input for two horizontal directions. Such a standard has also been applied to nuclear power generation facilities, which can be said to have the strictest aseismic design (Kim *et al*. 2004).

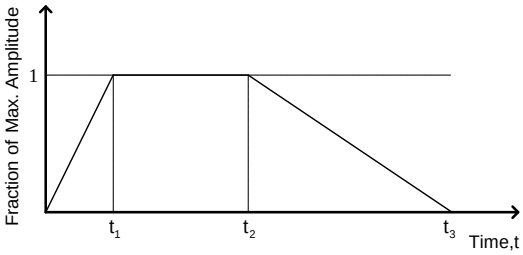

Fig. 7 Duration envelope function

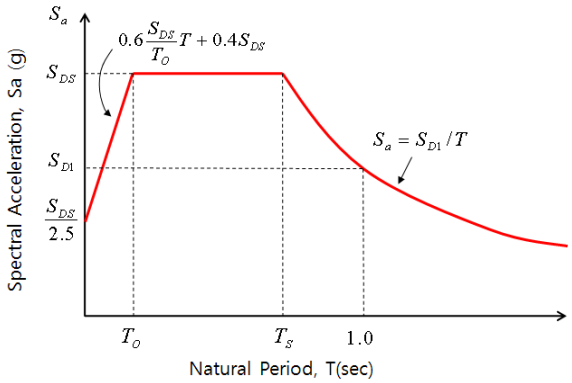

Fig. 8 Design response spectrum of KBC-2005

Table 1 Parameters of the duration enveloping function

Magnitude	Rise time (t_1)	Duration of strong motion (t_2–t_1)	Decay time (t_3–t_2)
7.0-7.5	2	13	9
6.5-7.0	1.5	10	7
6.0-6.5	1	7	5
5.5-6.0	1	6	4
5.0-5.5	1	5	4

$$\left|\rho_{ij}\right| = \left|\lim_{0\le\tau\le T_0} \rho_{ij}(\tau)\right| < 0.3 \tag{13}$$

$$\rho_{ij} = \frac{\sum_{m=1}^{N_i}\left(\ddot{x}_i(t_m)-\mu_i\right)\left(\ddot{x}_j(t_m-\tau)-\mu_j\right)}{\sqrt{\sum_{m=1}^{N_i}\left(\ddot{x}_i(t_m)-\mu_i\right)^2}\sqrt{\sum_{m=1}^{N_i}\left(\ddot{x}_J(t_m)-\mu_J\right)^2}} \tag{14}$$

The correlation coefficient $\rho_{ij}(\tau)$ between the artificial seismic wave $\ddot{x}_i(\tau)$ and $\ddot{x}_j(\tau)$ can be calculated using Eq. (14) because the two seismic wave time series follow the Gaussian probability distribution. Here, t_m=$m\Delta t$, and μ_i and μ_j are respectively, the average for the time axes of $\ddot{x}_i(\tau)$ and $\ddot{x}_j(\tau)$, and are generally 0. Table 2 lists the correlations of seven seismic waves generated previously, and the correlation coefficient of the generated artificial seismic waves all

Table 2 Correlation of artificial earthquakes

	1	2	3	4	5	6	7
1	1	-	-	-	-	-	-
2	0.0326	1	-	-	-	-	-
3	0.0585	0.0690	1	-	-	-	-
4	0.0007	0.0000	0.0963	1	-	-	-
5	0.0242	0.0220	0.0469	0.1246	1	-	-
6	0.0157	0.0607	0.0123	0.0768	0.1719	1	-
7	0.113	0.0177	0.0907	0.0353	0.0495	0.0850	1

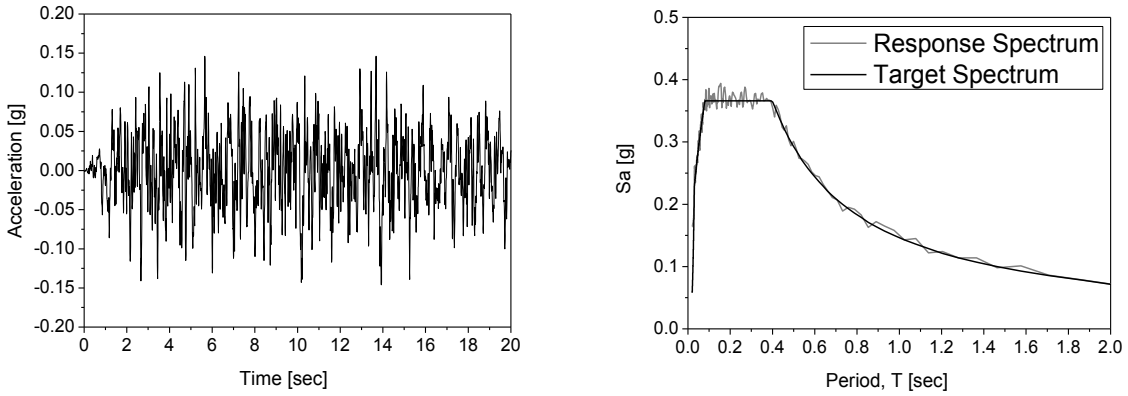

(a) Time history of artificial earthquake, PGA=0.15g (b) Target and response spectrum

Fig. 9 Artificial earthquake (Rock (S_B), Seismic area (1))

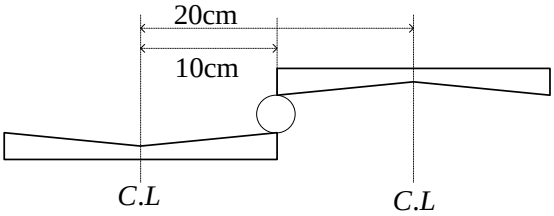

Fig. 10 Cross-section diagram of the CFPBS

appeared to be under 0.3. Therefore, the seven artificial seismic waves fulfill the aseismic design specifications of Korea.

4 Shaking table test

The CFPBS used in numerical analysis and the shaking table test was created with a cone-type friction surface, as shown in Fig. 10, and can control the acceleration response and displacement response to an earthquake using the slope of the friction surface. The upper structures cannot be balanced with just one single CFPBS. Therefore, the aseismic device comprised of 4 CFPBS's, as shown in the figure on the left of Fig. 1, was used in the shaking table test. The maximum load was

Fig. 11 CFPBS and censors arrangement for the shaking table test

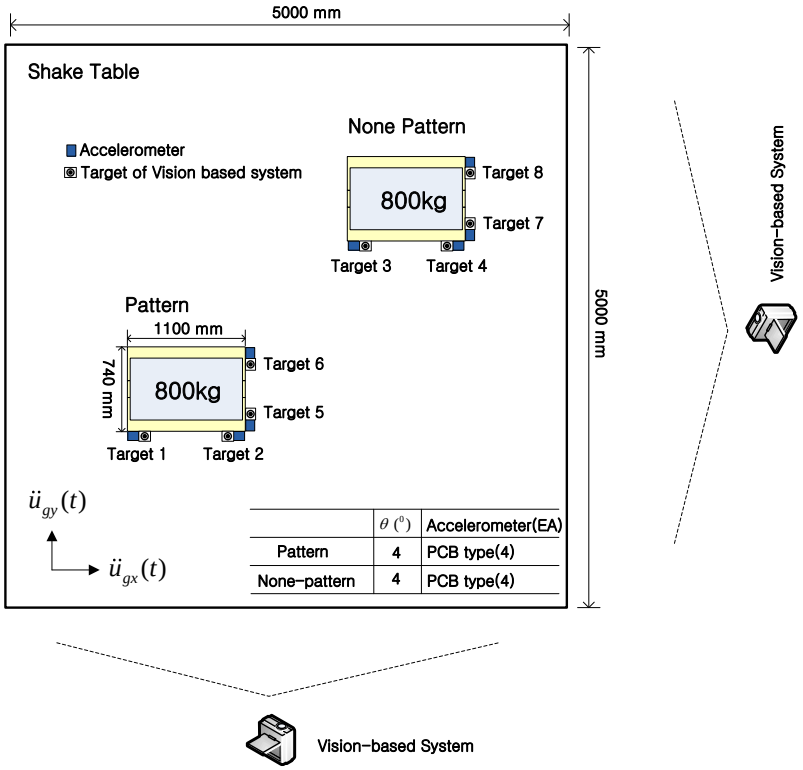

Fig. 12 CFPBS and accelerometers arrangement for the shaking table test

over 2000 kg, and the allowed displacement was 20 cm. The CFPBS was prepared with and without patterns on the friction surface, and the weight of the upper mass was set to 800 kg because the weight of the communication rack generally used is within 1000 kg. Concrete was placed within the rack to secure the mass to prevent the noise from internal impact during seismic input.

Four acceleration sensors were attached to the upper panel of the aseismic device, two each in two directions of the axes, and the CFPBS response acceleration by seismic motion was measured.

Table 3 Plan of the shaking table test

Load case	Details
1	· Ambient test using white noise signals · Uni-axial test (x direction)
2	· Artificial earthquake (scale up : ×1~3) · Uni-axial test (x direction)
3	· Artificial earthquake (scale up : ×1~3) · Bi-axial test (x ,y direction)
4	· El Centro(NS component, PGA=0.348g) · Uni-axial test (x direction)
5	· Kobe(NS component, PGA=0.835g) · Uni-axial test (x direction)
6	· Ambient test using white noise signals · Uni-axial test (x direction)

For convenience, the horizontal direction was defined as the *x*-axis and *y*-axis, respectively, in Fig. 12. The specimen comprised of the CFPBS aseismic device and an 800kg rack was arranged along the longitudinal *x*-axis of the rack, as shown in Figs. 11 and 12. The displacement was measured for both the *x*-axis and *y*-axis using a vision-based measurement system developed by Seong-Wan Kim, and a mobile digital camcorder was used as the sensor to measure the remote displacement response. The digital image correlation (DIC) technique was used for the digital image processing method, and image transform function (ITF) correcting the geometrical distortion between the modified image and non-modified image was applied to calculate below the unit pixel and determine the displacement response (Kim *et al*. 2012).

The shaking table test was performed on Shake table B, which is the triple-degree of freedom shake table system of the Seismic Simulation Test Center, Pusan University, and the order of execution is shown in Table 3. The seismic test by white noise for a single axis (*x*-axis) was performed to review the changes in the dynamic characteristics of CFPBS before/after the shaking table test. The CFPBS was expected to have the same performance for all horizontal directions because the friction surface was designed in the cone-type. The shaking table test was conducted using actually measured seismic waves of the El Centro NS and Kobe NS only with a single axis. On the other hand, as for an artificial seismic wave, the single-axis and double-axis were conducted to determine the influence of double-axis excitation on the response of CFPBS.

5 Results of shaking table test

5.1 Changed in dynamic characteristics due to shaking table test

To review the changes in the dynamic characteristics of CFPBS due to the shaking table test, the seismic test by white noise with a PGA of 0.1 g was conducted before the test, and after the test, the seismic test by the same white noise was conducted again without other changes to the specimen. Figs. 13 and 14 show the acceleration response of the CFPBS before/after the test in the power spectral density function through the ensemble average. According to the characteristics of

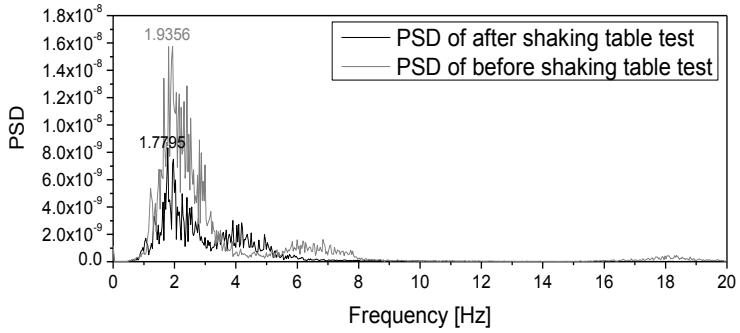

Fig. 13 PSD function of the none-patterned CFPBS from the ambient test

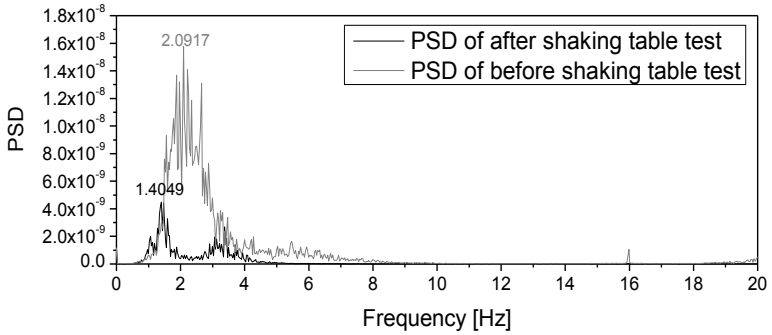

Fig. 14 PSD function of the patterned CFPBS from the ambient test

the CFPBS, where the specific frequency changes according to the location of the ball, the specific frequency does not appear around a certain frequency but changes from 1~10Hz. Regarding the none-patterned CFPBS, the tendency of the specific frequency distribution before/after the test was similar. Therefore, it appears that the cave-in phenomenon of the friction surface by the ball due to the effect of the upper mass did not have a significant effect on the changes in the dynamic characteristics of the CFPBS. For the patterned CFPBS, however, the cave-in phenomenon of the friction surface by the ball and upper mass changed the pattern and had a large influence on the dynamic characteristics of the CFPBS.

5.2 Response of shaking table test

The shaking table test was conducted in the order shown in Table 3, and the maximum values for each axial direction among the acceleration signals obtained from the acceleration sensor installed on the specimen and the input acceleration signal were compared with the results of numerical dynamic analysis of CFPBS. Figs. 15 and 16 present the PSD function of the CFPBS response acceleration signal during the vibration of an artificial seismic wave (Uni-axial test, PGA=0.25 g). The area of 0.5~10 Hz is believed to be the mode with a large contribution. The specific frequency of the CFPBS is concentrated around the low frequency area <4Hz because of the characteristics of the CFPBS with a certain slope that is not a pendulum. Therefore, the mode exceeding 10Hz was regarded as noise by the friction surface pattern and other environments, and a 10Hz low pass filter was applied to all response signals.

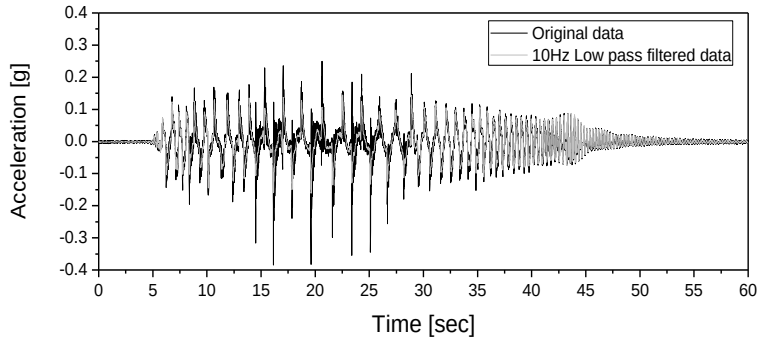

(a) Time history of the none-patterned CFPBS

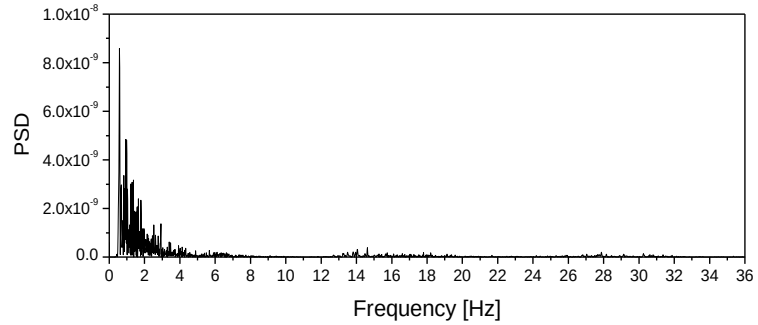

(b) PSD function

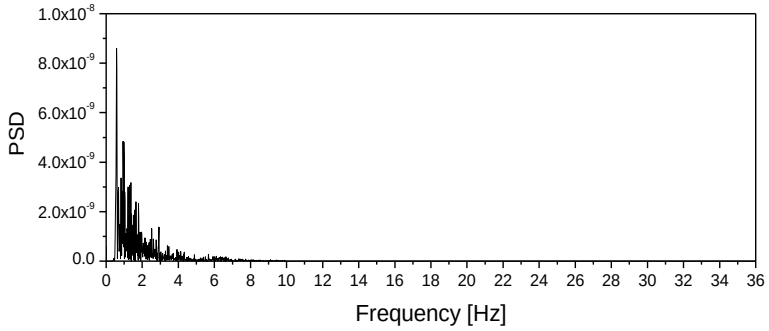

(c) 10Hz low pass filtered PSD function

Fig. 15 Response signals of the none-patterned CFPBS at an artificial earthquake uni-axial test, PGA=0.24 g

Table 4 lists the shaking table test results, and the Kobe NS seismic wave was not recorded exceeding the allowed displacement during the shaking table test. Table 4 shows that the CFPBS has weak seismic performance for small-sized earthquakes. On the other hand, for large-sized earthquakes, whose input seismic wave has a PGA over 0.3g, the CFPBS showed outstanding seismic performance with excellent response acceleration. Moreover, the response acceleration for the double-axis seismic test was found to be smaller. Tables 5 and 6 list the maximum displacement response signal measured using vision-based system for a single-axis seismic test and a double-axis seismic test, respectively. The displacement response increased in proportion to the PGA of the input seismic wave in all cases.

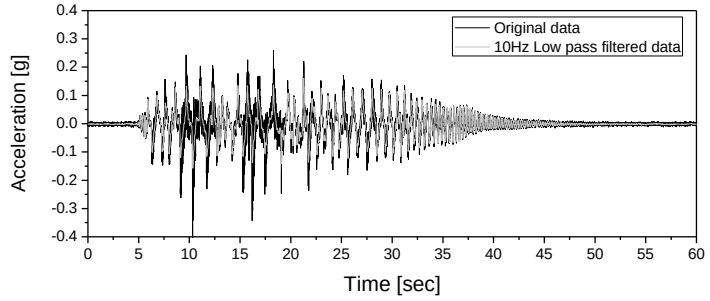

(a) Time history of the none-patterned CFPBS

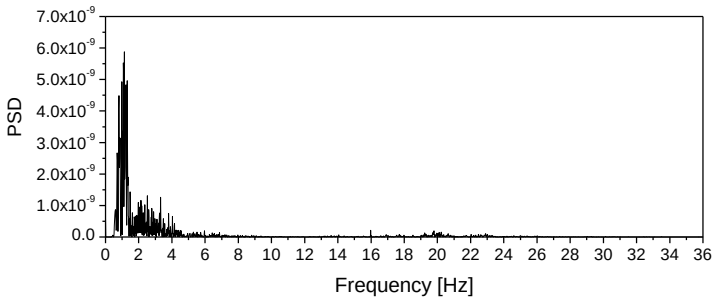

(b) PSD function

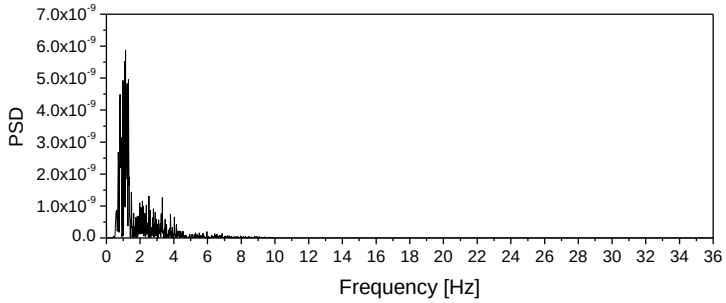

(c) 10Hz low pass filtered PSD function

Fig. 16 Response signals of patterned CFPBS at an artificial earthquake uni-axial test, PGA=0.24g

Table 4 Maximum response accelerations of the CFPBS by the shaking table tests (θ=4°, 10Hz low pass filtered signal)

	Peak Acceleration of Table motion [g]		Maximum response accelerations of CFPBS [g]			
			None-pattern		Pattern	
	Direction		Direction		Direction	
	X	*Y*	*X*	*Y*	*X*	*Y*
Artificial uni-axial×1	0.151	·	0.159	·	0.151	·
Artificial uni-axial ×1.5	0.242	·	0.161	·	0.152	·
Artificial uni-axial ×2	0.321	·	0.178	·	0.159	·
Artificial uni-axial ×2.5	0.401	·	0.121	·	0.153	·

Table 4 Continued

Artificial uni-axial ×3	0.481	·	0.183	·	0.181	·
Artificial bi-axial ×1	0.161	0.159	0.161	0.229	0.111	0.138
Artificial bi-axial ×1.5	0.242	0.242	0.129	0.188	0.152	0.211
Artificial bi-axial ×2	0.322	0.321	0.092	0.121	0.13	0.19
Artificial bi-axial ×2.5	0.402	0.401	0.071	0.042	0.102	0.132
Artificial bi-axial ×3	0.479	0.48	0.071	0.061	0.101	0.093
El Centro NS	0.348	·	0.062	·	0.141	·

Table 5 Maximum response displacements of the CFPBS by uni-axial shaking table tests

	Peak Acceleration of Table motion [g]	Maximum Response Displacements of CFPBS [cm]			
		Pattern		None-pattern	
		X (target 2)	*Y*	*X* (target 4)	*Y*
Artificial uni-axial×1	0.151	5.655	·	6.661	·
Artificial uni-axial×1.5	0.242	8.393	·	6.334	·
Artificial uni-axial×2	0.321	10.272	·	11.285	·
ElCentro NS	0.348	13.102	·	15.741	·
Artificial uni-axial×12.5	0.402	15.487	·	17.187	·
Artificial uni-axial×13	0.479	17.590	·	14.856	·
Kobe NS	0.835	18.789	·	17.790	·

Table 6 Maximum response displacements of the CFPBS by bi-axial shaking table tests

	Peak Acceleration of Table motion [g]		Maximum Response Displacements of CFPBS [cm]			
			Pattern		None-pattern	
			X (target 2)	*Y* (target 5)	*X* (target 4)	*Y* (target 7)
Artificial bi-axial ×1	0.161	0.159	5.106	4.432	6.263	5.006
Artificial bi-axial ×1.5	0.242	0.242	5.548	1.931	6.015	6.241
Artificial bi-axial ×2	0.322	0.321	9.278	13.104	8.026	9.267
ElCentro NS	0.348	·	13.071	·	15.822	·
Artificial bi-axial ×2.5	0.402	0.401	10.408	12.296	8.517	10.636
Artificial bi-axial ×3	0.479	0.48	13.429	14.461	11.057	13.459
Kobe NS	0.835	·	18.895	·	18.243	·

6. Results of numerical analysis

6.1 Characteristics of CFPBS

The response signal of numerical dynamic analysis determined by substitution of an arbitrary μ_r and the response signal obtained from the free vibration test conducted by changing the upper

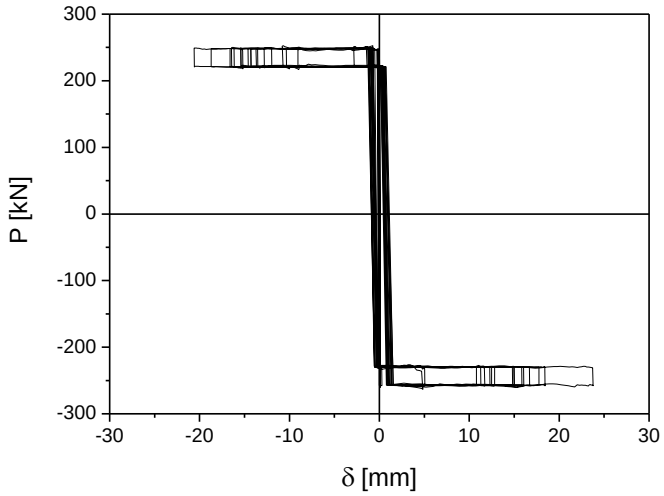

Fig. 17 P-δ curve of CFPBS response with El Centro(NS component, 1940) at μ_r=0.004, θ=4°

mass of the CFPBS were compared to predict μ_r according to the changes in the upper mass. Numerical dynamic analysis was performed using μ_r.

Fig. 17 shows the P-δ curve of the CFPBS for the El Centro NS seismic wave, and the displacement characteristics can be found. CFPBS does not protect the structure from earthquakes by dissipating the seismic energy, but uses the slope and friction to change the specific frequency of the structure and determine the response acceleration. Therefore, its ability to dissipate the seismic energy is limited, and there are some break points due to the cone-type friction surface.

Fig. 18 presents the maximum acceleration response of the ball structure as a function of μ_r and the angle of inclination θ of CFPBS when numerical analysis was conducted using each seismic wave. Fig. 19 shows the maximum displacement response in the same situation. The CFPBS showed the same acceleration response once μ_r and θ were determined for different input seismic waves. At a low μ_r, the CFPBS increases linearly, and for a higher μ_r, the slope decreased slightly but did not have a large effect on the overall linearity, which can be seen from Fig. 18. Fig. 19 shows the arrangement of the maximum displacement response of the CFPBS according to the slope and μ_r for each seismic wave, and Fig. 19 (a) and (b) presents cases of actual seismic waves with a large energy. Among them, in the case of the El Centro NS seismic wave, it exceeded the allowable displacement for a low μ_r, but when a mass over a certain amount was placed over the upper panel, μ_r increased to fulfill the allowable displacement. On the other hand, for the Kobe NS seismic wave with the largest seismic wave energy, it exceeds the allowable displacement in most cases. For artificial seismic waves with small energy, it fulfills the standards in all cases, as shown in Fig. 19 (c).

6.2 Calculation of the response acceleration reduction rate of CFPBS using a numerical analysis program

The CFPBS reduction rate γ was defined as the ratio of the PGA and CFPBS maximum acceleration response, as expressed in Eq. (15). Fig. 20 shows the attenuation rate when the PGA

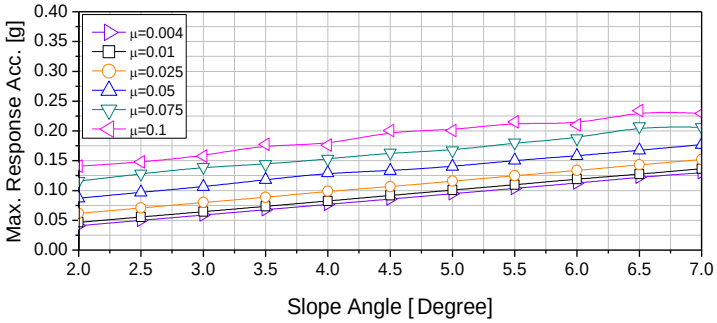

(a) El Centro (NS component, 1940)

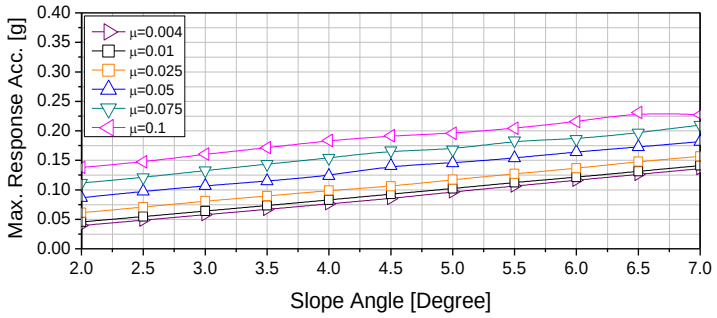

(b) Kobe (NS component, 1995)

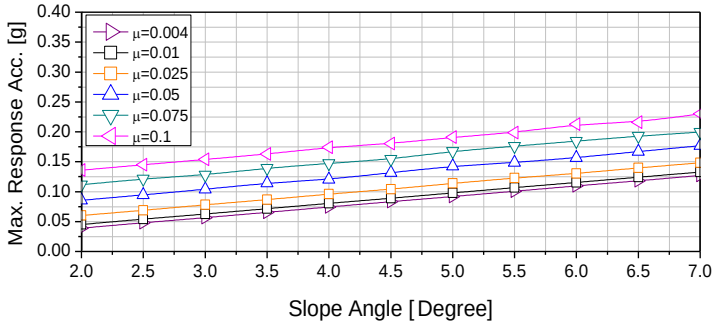

(c) Artificial earthquake

Fig. 18 Maximum response accelerations based on μ_r and θ

was amplified while fixing θ to 4° for each seismic wave. The μ_r value was taken arbitrarily to be 0.004, 0.007 and 0.011. For each seismic wave, the CFPBS maximum acceleration response was determined from numerical analysis. Eq. (15) was used to arrange the reduction rate. The CFPBS reduction rate with the same performance appears to be a single exponential function according to the size of μ_r regardless of the size of the seismic wave.

$$\gamma = \left(1 - \frac{a_{\max,CFPBS}}{\ddot{u}_{g,\max}}\right) \times 100 \tag{15}$$

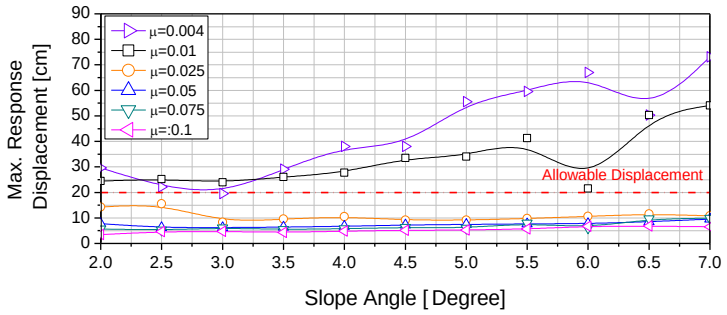

(a) El Centro(NS component, 1940)

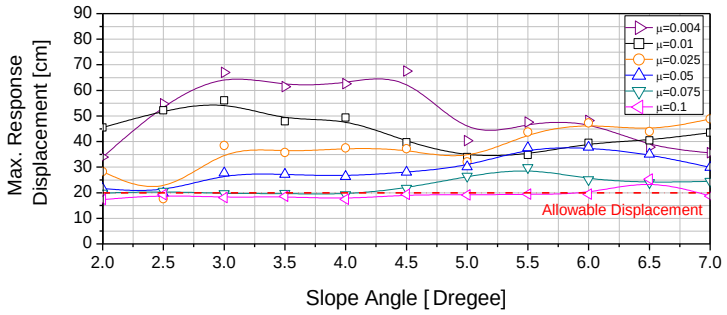

(b) Kobe(NS component, 1995)

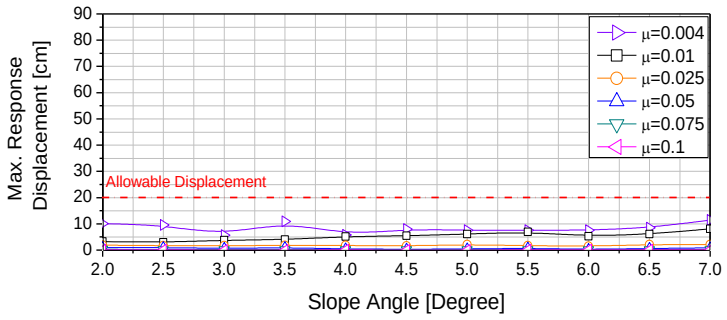

(c) Artificial earthquake

Fig. 19 Maximum response displacements based on μ_r and θ

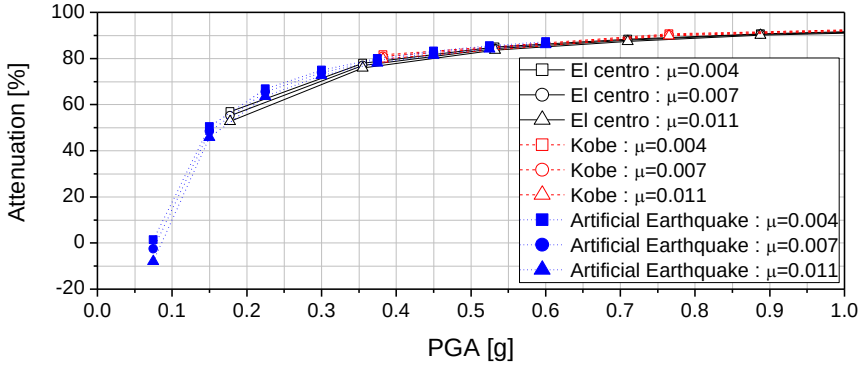

Fig. 20 Attenuation rate when the PGA was amplified while fixing θ to 4°

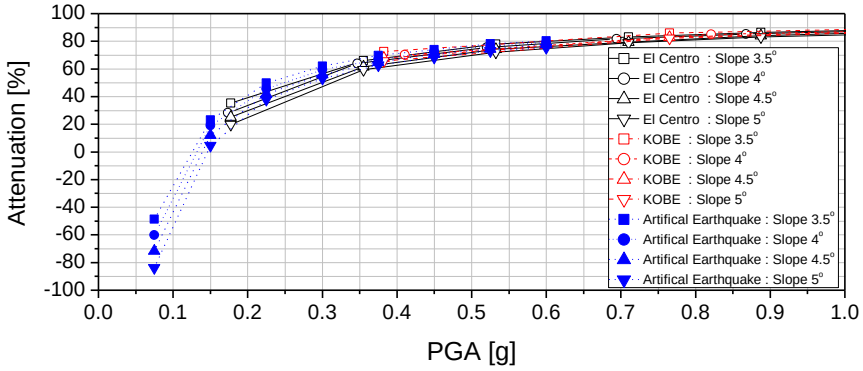

Fig. 21 Attenuation rate when the PGA was amplified while fixing μ_r to 0.05

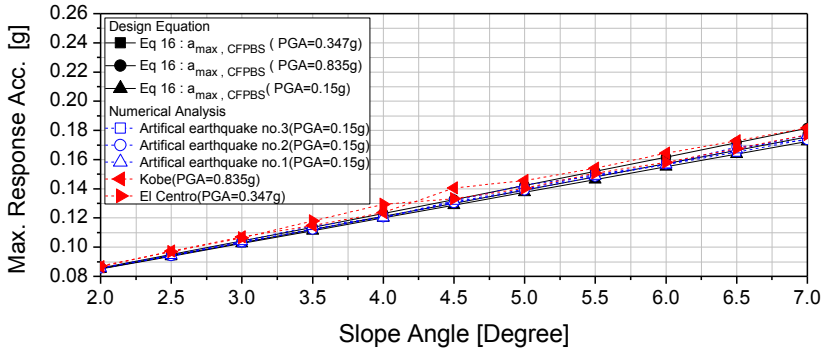

Fig. 22 Maximum response acceleration comparison of the design equation and numerical analysis (μ_r=0.05)

Figs. 18, 20 and 21 confirmed that decreases in θ or μ_r reduce the maximum acceleration. The maximum displacement response decreases at higher μ_r, and θ does not have a very large influence. Fig. 18 shows that CFPBS used in this study was designed to have a maximum acceleration response converging to approximately 0.075g for the input seismic wave in the case of μ_r was 0.01. The aseismic design specifications of domestic civil infrastructure are 0.154 g, and the PGA of an artificial seismic wave fulfilling the Korean Building Code-Structural (KBC-2005) is approximately 0.15 g. Therefore, the maximum acceleration response of the CFPBS used in this study converging to 0.075 g indicates that the reduction rate for the PGA of an artificial seismic wave fulfilling the Korean Building Code-Structural (KBC-2005) is approximately 45%, as shown in Fig. 18. Therefore, the reduction rate is satisfactory against the standards used in the aseismic design of domestic infrastructure. The reduction performance of the CFPBS improved with increasing PGA of the input seismic wave (Figs. 20 and 21).

7. Design equation of the CFPBS

Eq. (16) was used as the design equation to determine the maximum acceleration response of the upper panel of CFPBS. Eq. (16) was suggested by Tsai *et al*. (2007) for rolling-type seismic isolation bearings. To compare with the response of numerical analysis performed previously, the

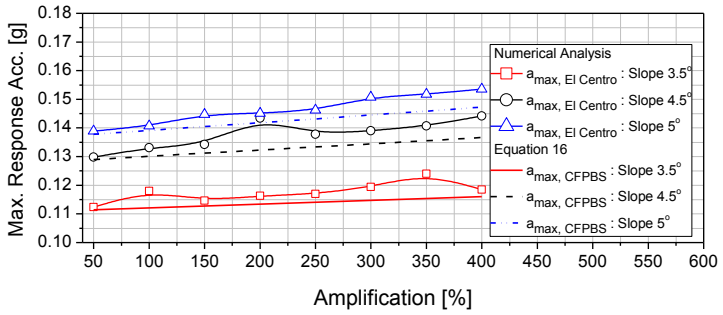

(a) El Centro(NS component, 1940)

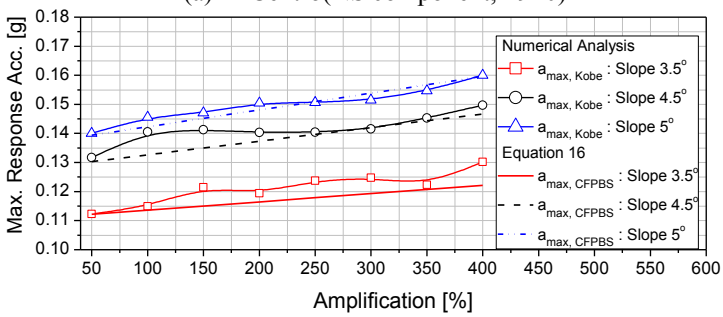

(b) Kobe(NS component, 1995)

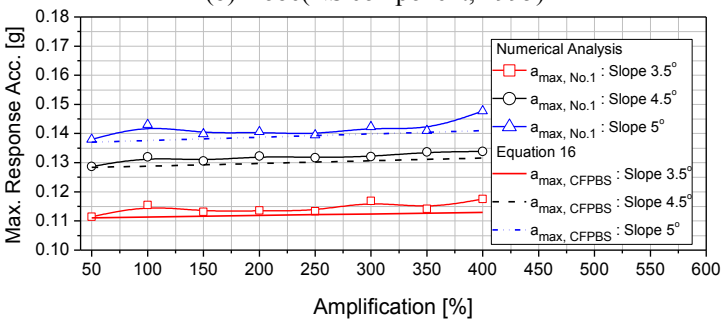

(c) Artificial earthquake

Fig. 23 Maximum acceleration response of the CFPBS by amplifying the PGA of each seismic wave (Artificial earthquake uni-axial test, PGA=0.25 g, μ_r=0.05)

PGA (Peak Ground Acceleration) $\ddot{u}_{g,\max}$ value was set to 0.15 g, 0.347 g and 0.821 g, which are the PGA values for the artificial seismic wave created in this study, El Centro NS, and Kobe NS, respectively, and μ_r was substituted arbitrarily with 0.05. By formalizing the relationship between the slope and maximum acceleration response of the CFPBS, Fig. 22 shows that the response calculated from Eq. (16) and the response determined by numerical analysis are similar.

$$a_{\max,CFPBS} = \cos^2\theta(\mu_r + \tan\theta)(g + \ddot{u}_{g,\max}\tan\theta) \tag{16}$$

Fig. 23 shows the calculation of the maximum acceleration response of CFPBS through numerical analysis by amplifying the PGA of each seismic wave by 0.5~4 fold. Here, μ_r was fixed to 0.05. Eq. (16) only considered the PGA of the seismic wave but did not consider the energy of the seismic wave. Therefore, the maximum acceleration response of the CFPBS considering the

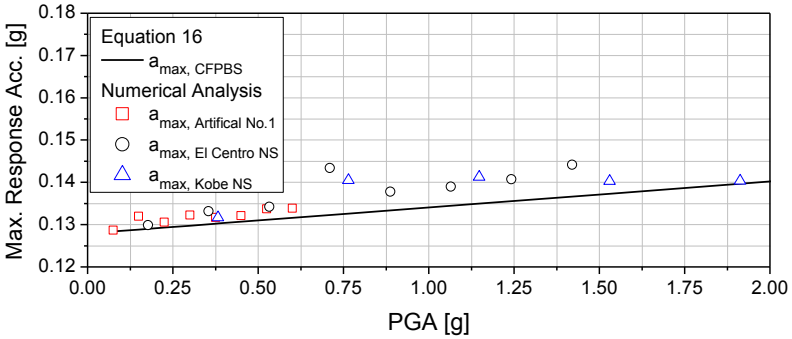

Fig. 24 Comparison of the maximum response acceleration of the design equation and numerical analysis by amplifying PGA(μ_r=0.05, θ=4.5°)

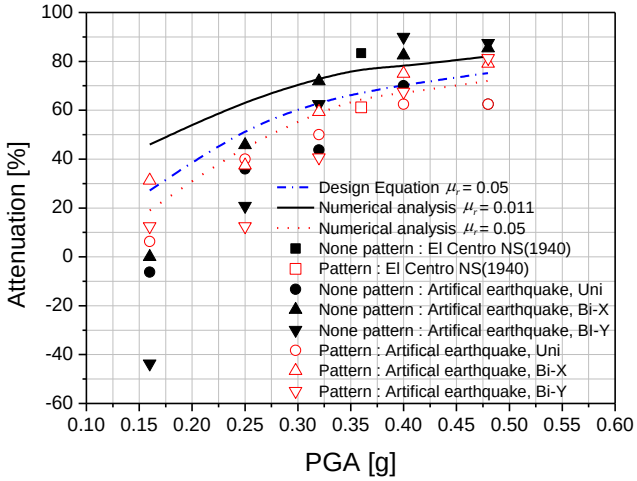

Fig. 25 Comparison of the attenuations from numerical analysis and the shaking table test

energy of the seismic wave was determined by conducting numerical analysis with an actual seismic wave PGA amplified in multiples. As shown in Fig. 23(c), for the artificial seismic wave with a small amount of energy, the numerical analysis results largely coincide with the results of the equation, but there were some differences observed for an actually measured seismic wave of (a) and (b). The responses in Fig. 23 were organized not by multiples but by the PGA, as shown in Fig. 24. As the seismic wave is amplified, the maximum acceleration response of the CFPBS converges at approximately 0.14 g, which is similar to the results shown in Figs. 18 and 22. On the other hand, the angle of inclination θ was 4.5°, and μ_r was 0.05. Seismic waves mostly have a PGA below 1 g, so it appears that Eq. (16) can be used as the design equation of the CFPBS.

8. Comparative analysis of the results between numerical analysis and shaking table test

The acceleration data obtained from shaking table test in Table 4 was converted to the reduction

rate μ_r by Eq. (15). Fig. 25 compares the reduction rate obtained from numerical dynamic analysis and the design equation. The Kobe NS seismic wave beyond the allowed displacement was excluded. The none-patterned CFPBS showed better seismic control performance than the patterned CFPBS for earthquakes over 0.3 g, and was similar to the numerical dynamic analysis results. On the other hand, for a low-level earthquake, the tendencies vary so that the response acceleration appears to be largely amplified thus being weak. The CFPBS with a pattern on the friction surface shows more than 60% of the reduction rate for an input seismic wave over 0.3 g of the PGA, and appears similar to the reduction rate of the design equation and numerical dynamic analysis result of case of μ_r was 0.05

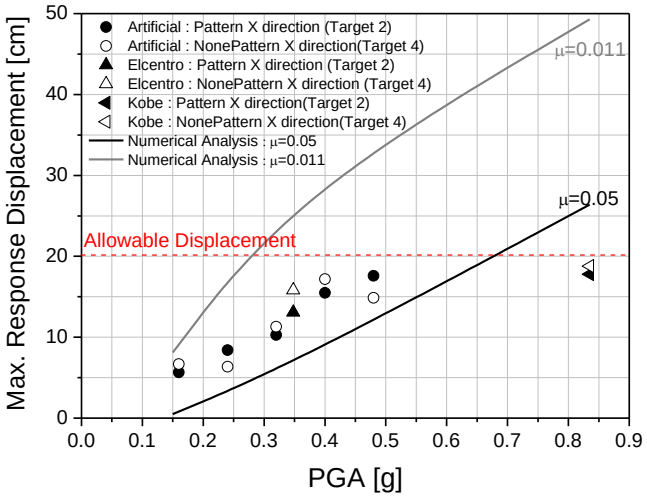

Fig. 26 Comparison of the maximum response displacements from numerical analysis and the uni-axial shaking table test

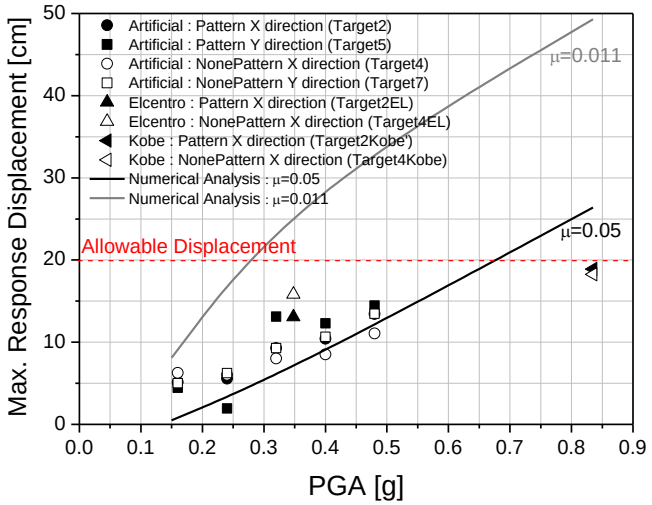

Fig. 27 Comparison of the maximum response displacements from numerical analysis and the bi-axial shaking table test

Fig. 26 compares the maximum displacement response of CFPBS calculated from numerical analysis and the maximum displacement response measurement from the single-axis shaking table test. μ_r was assumed to be 0.011 for the none-patterned CFPBS and 0.05 for the patterned CFPBS just like Fig. 25. The none-patterned CFPBS did not coincide with case of μ_r was 0.011, and was similar to the case of 0.05. Regardless of the existence of the pattern, the response displacement of the CFPBS showed a similar tendency, μ_r was 0.05, but was approximately 5mm greater. Fig. 27 compares the maximum displacement response of the CFPBS calculated by numerical analysis and the maximum displacement response measured using the double-axis shaking table test. Excluding the case of the El Centro NS seismic wave, the maximum displacement response showed a similar tendency to the case of μ_r was 0.05. That is, the patterned CFPBS has a similar acceleration and displacement to those of the response of numerical analysis. Therefore, if μ_r can be inferred accurately, the CFPBS with frictional capability on the friction surface can determine the seismic performance of the CFPBS without undergoing a complex process, such as tests and numerical analysis, using the design equation.

9. Conclusions

In this study, the motion equation of the CFPBS (Cone-type Friction Pendulum Bearing System) was derived, and the Newmark-β method was used to prepare a MATLAB 7.0-based numerical analysis program. The design equation that can determine the acceleration response of CFPBS was reviewed, and the parameter study and shaking table tests were conducted to confirm the validity of the design equation and seismic performance for the horizontal direction.

The reduction performance of the CFPBS decreased by increasing μ_r. But when the μ_r is less than 0.01, the range of the change in maximum acceleration response was small.

The rate of CFPBS reduction with the same performance appears in the form of a single exponential function according the size, regardless of the type of seismic wave. The reduction performance of the CFPBS increased with increasing magnitude of the seismic wave.

The response acceleration signal obtained from the shaking table test was estimated to include the noise from the patterns and the breakpoint occurring from the cone-shaped friction surface. Therefore, the mode over 10 Hz was estimated to be noise due to other environments and the pattern of the friction surface, and a 10 Hz low pass filter was applied to all response signals.

An analysis of the response acceleration signal measured from the shaking table test showed that both the displacement response and reduction rate of the acceleration response could not be relied upon for none-patterned CFPBS. The patterned CFPBS, however, showed a similar trend of the displacement response and reduction rate obtained from the shaking table test, design equation and numerical analysis. Therefore, the CFPBS algorithm and design equation approached theoretically are reliable.

Acknowledgments

This work was supported by the energy efficiency & resources of the Korea Institute of Energy Technology Evaluation and Planning (KETEP) grant funded by the Korea government Ministry of Knowledge Economy (No. 2011T100200080). And special thanks to Mr. Jung in Entire Safe System for supporting equipments.

References

American Society of Civil Engineers (1999), *Seismic Analysis of Safety-Related Nuclear Structures and Commentary*, ASCE 4-98, Reston, VA, USA.

Architectural Institute of Korea (2005), Korea Building Code-Structural, Kimoondang, Seoul, Korea.

Hwang, I.H., Shin, H.J. and Lee, J.S. (2008), "Base isolation performance of friction pendulum system using magnetic force", *J. Earthq. Eng. Soc. Korea*, **12**(4), 55-66.

Jang, J.B., Kim, J.K., Hwang, K.M., Ham, K.W., Park, J.W. and LEE, C.W. (2008), "Experimental Study of Friction Pendulum System to Improve the Seismic Capacity of Transformer", *J. Earthq. Eng. Soc. Korea*, **12**(2), 1-8.

Japan Electric Association (1999), *The Guideline of Earthquake-proof Design Method for Substation Electric Equipment*, JEAG 5003, Tokyo, Japan.

Jeon, B.G., Jang, S.J., Park, K.R. and Kim, N.S. (2011), "Seismic Performance Evaluation of Cone-type Friction Pendulum Bearing System", *J. Earthq. Eng. Soc. Korea*, **15**(2), 23-33.

Kasalanati, A., Reinhorn, A.M., Constantinou, M.C. and Sanders, D. (1997), "Experimental study of ball-in-cone isolation system", *Proceedings of the Structures Congress XV(*ASCE), Portland, Oregon, April, **2**, 1191-1195

Kesti, M.G., Mowrtage, W. and Erdik, M. (2010), "Earthquake risk reduction of structures by a low-cost base isolation device: experimental study on BNC bearings", *14th European Conference on Earthquake Engineering*, Ohrid, Macedonia, August.

Kim, N.S., Kim, J.M. and LEE, G.H. (2004), *A Study on Artificial Earthquake Generation for Time History Analysis of Seismically Isolated Bridge*, Institute for Research and Industry Cooperation in PNU, Busan, Korea.

Kim, S.W. and Kim, N.S. (2012), "Application of vision-based measurement system for estimation of dynamic characteristics on hanger cables", *Korean Soc. Civil Eng.*, **32** (1-A), 1-10.

Krishnamoorthy, A. (2013), "Effect of soil-structure interaction for a building isolated with FPS", *Earthq. Struct.*, **4**(3), 285-297.

Lee, G.C., Liang, Z. and Niu, T.C. (2003), *Seismic Isolation Bearing*, US2003/0099413 A1, US Patent application publication, Alexandria, Virginia, USA.

Lin, T.W. and Hone, C.C. (1993), "Base isolation by free rolling rods under basement", *Earthq. Eng. Struct. Dyn.*, **22**(4), 261-273.

Mokha, A., Constanitinou, M.C. and Reinhorn, A.M. (1990), *Experimental Study and Analytical Prediction of Earthquake Response of Sliding Isolation System with a Spherical Surface*, Report No. NCEER-90-0020, National Center for Earthquake Engineering Research, State University of New York, Bufflo, New York, USA.

Murota, N., Feng, M.Q. and Liu, G.Y. (2005), *Experimental and Analytical Studies of Base Isolation System for Seismic Protection of Power Transformers*, MCEER-05-0008, Multidisciplinary Center for Earthquake Engineering Research, State University of New York, Bufflo, New York.

Nacamuli, A.M. and Sinclair, K.M. (2011), "Seismic isolation: applications of work safe technologies ball-N-cone isolator", *Proceedings of the Structural Congress (ASCE),* Las Vegas, NV, April.

Sevket, A. (2012), "Investigation of effectiveness of double concave friction pendulum bearings". *Comput. Concrete*, **9**(3), 195-213.

Tsai, M.H., Wu, S.Y., Chang, K.C. and Lee, G.C. (2007), "Shaking table test of a scaled bridge model with rolling-type seismic isolation bearings", *Eng. Struct.*, **29**(5), 694-702.

Wu, S.Y., Lee, S.N., Tsai, M.H. and Chang, K.C. (2004), "Seismic isolation tests of a bridge model using rolling type seismic isolation bearings", *Proceeding of the 17th KKCNN symposium on civil engineering*, Ayutthaya, Thailand**,** December.

Zayas, V., Low, S.S. and Mahin, S.A. (1987), *The FPS Earthquake Resisting System*, Experimental Report, Report No. UCB/EERC-87/01, Earthquake Engineering Research Center, University of California, Berkeley, USA.